Bioelectrochemistry 105 (2015) 25–33

Contents lists available at ScienceDirect

Bioelectrochemistry

journal homepage: www.elsevier.com/locate/bioelechem

Stability, redox parameters and electrocatalytic activity of a cytochrome domain from a new subfamily

María F. Molinas, Leandro Benavides, María A. Castro, Daniel H. Murgida *

Departamento de Química Inorgánica, Analítica y Química Física and INQUIMAE (CONICET-UBA), Facultad de Ciencias Exactas y Naturales, Universidad de Buenos Aires, Ciudad Universitaria, Pab. 2, piso 1, C1428EHA Buenos Aires, Argentina

ARTICLE INFO

Article history:
Received 20 January 2015
Received in revised form 21 April 2015
Accepted 3 May 2015
Available online 6 May 2015

Keywords:
Heme proteins
Iron–sulfur proteins
Protein electron transfer
Hydrogen peroxide sensing
SERR spectroelectrochemistry

ABSTRACT

We report a spectroscopic, electrochemical and spectroelectrochemical characterization of the soluble cytochrome *c* domain (Cyt-D) from the *Rhodothermus marinus* caa_3 terminal oxygen reductase and its putative electron donor, a high potential [4Fe–4S] protein (HiPIP). Cyt-D exhibits superior stability, particularly at the level of the heme pocket, compared to archetypical cytochromes in terms of thermal and chemical denaturation, alkaline transition and oxidative bleaching of the heme, which is further increased upon adsorption on biomimetic electrodes. Therefore, this protein is proposed as a suitable building block for electrochemical biosensing. As a proof of concept, we show that the immobilized Cyt-D exhibits good electrocatalytic activity towards H_2O_2 reduction. Relevant thermodynamic and kinetic electron transfer parameters for Cyt-D and HiPIP are also reported, including reorganization energies of 0.33 eV and 0.42 eV, respectively.

1. Introduction

C-type monoheme cytochromes are mostly small soluble proteins involved in respiratory and photosynthetic electron transport chains [1–3]. In eukaryotes cytochrome *c* (Cyt-c) shuttles electrons from the bc_1 complex to the terminal respiratory enzyme in the inner mitochondrial membrane, a heme–copper oxygen reductase and, in addition, it plays a crucial role in apoptosis [4–6].

A common feature to all cytochromes *c* is that the heme prosthetic group is covalently attached to the protein via two thioether bonds to cysteine residues that usually present a CXXCH motif, with the histidine residue acting as one of the axial ligands of the heme iron. The other axial position is most often occupied by a methionyl ligand, leading to a six-coordinated low spin complex, but can also remain either vacant or coordinated by other amino acids such as histidine, cysteine or lysine [1,3,7].

Class I cytochromes represent a large group of single domain low-spin C-type heme proteins that, according to sequence, phylogeny and function, have been classified into 16 subclasses. All members of the family present a fold that includes a minimum of three α helices arranged around the heme group, and further less conserved structural elements [7,8].

In addition to the soluble electron shuttles, C-type cytochromes may also be part of larger redox enzymes and, moreover, heme *c* containing protein domains can also be found fused to other domains. This is the case of the caa_3 terminal oxygen reductase from *Rhodothermus marinus*, a Gram-negative strict aerobe thermophile bacterium [9–14]. This enzyme belongs to the A2 subfamily of oxygen reductases. As in the mammalian counterparts, the catalytic site of the *R. marinus* enzyme is constituted by a binuclear heme a_3–Cu_B center located in the subunit I. The main difference refers to subunit II which, in addition to the canonical Cu_A site, contains a cytochrome *c* domain (Cyt-D) in the C-terminus that has been suggested as the primary acceptor of electrons transported by the putative donor, a periplasmic high-potential iron–sulfur protein (HiPIP) [9–14]. Cyt-D has been overexpressed in *Escherichia coli*, yielding a well folded and stable soluble protein that retains the spectroscopic and redox properties of the domain in the holoenzyme [15–17].

The structure of Cyt-D has been solved at 1.3 Å resolution, revealing a heme group covalently linked to cysteines 16 and 19 and buried into the protein matrix, exposing only partially the substituent of ring C to the solvent. Methionine 74 and histidine 20 are the axial ligands of the six-coordinated low spin heme iron. The secondary structure comprises three relatively long and two short α-helices, two antiparallel β-strands that are connected by random coil segments forming a small β-sheet, and two extended loops. A comparison of the amino acid sequences of Cyt-D and other monoheme cytochromes from all known families shows similarities only with the C-fragments of caa_3 oxygen reductases, thus revealing a new subfamily of cytochromes distinct from the archetypical C-type proteins [15].

Abbreviations: Cyt-D, soluble cytochrome *c* domain of the caa_3 O_2-reductase from *R. marinus*; HiPIP, high potential iron–sulfur protein; TR-SERR, time-resolved surface-enhanced resonance Raman; GuHCl, guanidine hydrochloride.

* Corresponding author.
E-mail address: dhmurgida@qi.fcen.uba.ar (D.H. Murgida).

http://dx.doi.org/10.1016/j.bioelechem.2015.05.005
1567-5394/

In recent work we have investigated the electron transfer (ET) dynamics of Cyt-D in biomimetic complexes by employing a novel combination of experimental and computational methods that allowed for the identification of the most likely electron entry and exit points of Cyt-D, as well as for the interaction domains with the redox partner proteins [17].

Here we report crucial thermodynamic and kinetic redox parameters of Cyt-D and its putative electron donor HiPIP [18]. We also assess the stability of Cyt-D towards thermal and chemical denaturation, alkaline transitions and bleaching by reactive oxygen species. It is shown that, in general terms, this protein is characterized by higher stability than canonical counterparts such as horse heart Cyt-c and, therefore, it appears as a promising building block for the construction of bioelectronics devices. As a proof of concept, we tested the electrocatalytic activity of Cyt-D immobilized on biocompatible electrodes towards hydrogen peroxide reduction (pseudoperoxidase activity).

2. Experimental section

2.1. Chemicals

4-Mercapto-1-butanol (C_4-OH), 1-butanethiol (C_3-CH_3), 6-mercapto-1-hexanol (C_6-OH), 1-hexanethiol (C_5-CH_3), 8-mercapto-1-octanol (C_8-OH), 1-octanethiol (C_7-CH_3), 11-mercapto-1-undecanol (C_{11}-OH), 1-undecanethiol (C_{10}-CH_3), 16-mercapto-1-hexadecanol (C_{16}-OH), 1-hexadecanethiol (C_{15}-CH_3), 16-mercaptohexadecanoic acid (C_{15}-COOH), N-cyclohexyl-N′-(2-morpholinoethyl) carbodiimide metho-p-toluenesulfonate (CMC) and N-hydroxysuccinimide (NHS) were purchased from Sigma-Aldrich. Eicosane-1-thiol (C_{19}-CH_3) and 20-mercaptoeicosan-1-ol (C_{20}-OH) were synthesized and purified as described before [17]. Hydrogen peroxide was purchased from Mallinckrodt Baker Inc. All reagents were of the highest available purity and used without further purification. Solutions were prepared with deionized water ($R \geq 18$ MΩ; Millipore).

2.2. Proteins

The protocols for protein expression and purification have been described in detail elsewhere. Briefly, Cyt-D and HiPIP were obtained by expression in *E. coli* cells, followed by cell breaking in a French press, ultracentrifugation and thorough chromatographic purification [15,18].

2.3. Raman experiments

Resonance Raman (RR) spectra were acquired employing a confocal microscope coupled to a single stage spectrograph (Jobin Yvon XY) equipped with a 1800 L/mm grating and liquid nitrogen cooled back illuminated CCD detector. Elastic scattering was rejected with Notch filters. The 413 nm line of a cw. krypton ion laser (Spectra Physics BeamLok 2060) was focused onto the surface of a quartz rotating cuvette containing the sample by means of a long working distance objective (20×; N.A. 0.35). Typically, experiments were performed with laser powers of ca. 2 mW at the sample and acquisition times between 2 and 10 s.

Silver ring working electrodes for surface-enhanced resonance Raman (SERR) spectroelectrochemistry were polished and subjected to oxidation–reduction cycles to create a SERR-active surface, as previously described [19]. The electrodes were incubated into ethanolic solutions of the corresponding alkanethiol mixtures (ca. 1 mM total concentration) overnight to produce self-assembled monolayers (SAMs), rinsed and transferred to the spectroelectrochemical cell. The SERR spectroelectrochemical cell has been described before [19]. It contains a Pt wire and a Ag/AgCl (3.5 M KCl) electrode as counter and reference electrodes, respectively. During SERR measurements the working electrode was rotated at ca. 5 Hz to avoid laser-induced sample degradation. The electrolyte solution was 12.5 mM phosphate buffer (PBS), pH 7.0; 12.5 mM K_2SO_4. Protein adsorption was achieved by 15 minute incubation of the SAM-coated electrode in the SERR cell containing approximately 0.1 μM Cyt-D in the working electrolyte, at −400 mV. SERR spectra were measured in back-scattering geometry.

For time-resolved (TR-SERR) experiments, potential jumps of variable height and duration were applied to trigger the reaction. The SERR spectra were measured at variable delay times after each jump [20]. Synchronization of potential jumps and measuring laser pulses was achieved with a four channel pulse-delay generator (BNC-565) and a home-made pulse amplifier. The measuring pulses were generated by passing the cw laser beam through two consecutive laser intensity modulators (Linos Photonics). After background subtraction the spectra were treated by component analysis in which the spectra of the individual species were fitted to the measured spectra using home-made analysis software. The time resolution of the set-up is determined by the time constant of the electrochemical cell, which has been determined ca. 100 μs for the typical experimental conditions reported throughout this work.

2.4. Electrochemical measurements

Cyclic voltammetry (CV) and chronoamperometric experiments were performed either with a potentiostat/galvanostat PAR model 263A or with a Gamry REF600 electrochemical workstation, using a jacketed single compartment electrochemical cell (Dr. Bob's cell, Gamry) under Ar and contained inside a Faraday cage (Vista Shield, Gamry). As working electrodes we employed either home-made gold bead electrodes (1 mm diameter) or 3 mm diameter alumina-polished Au disk electrodes (Gamry). The system is completed with a Pt wire counter electrode and an Ag/AgCl (3.5 M KCl) reference electrode to which all potentials reported in this work are referred. The home-made working electrodes were cleaned by first annealing, then performing an oxidation at 2 V in 1 M $HClO_4$ and were finally treated in an ultrasonic pool for about 30 min. To remove residual adsorbed impurities, all electrodes were subjected to 30 voltammetric cycles between −0.2 and 1.6 V at 0.3 V/s in 1 M $HClO_4$. The surfaces of the clean electrodes were modified by overnight incubation into 1 mM ethanolic solutions of the desired alkanethiols. The SAM-coated electrodes were thoroughly washed with ethanol and water, subjected to 20 voltammetric cycles between −0.3 and 0.3 V at 0.3 V/s in PBS pH 7 and then incubated overnight into 200 μM solutions of Cyt-D for protein adsorption (PBS pH 7).

2.5. UV–vis absorption

UV–visible absorbance spectra were recorded on a Thermo Scientific Evolution Array spectrophotometer using 1.0 nm spectral bandwidth. Unless stated otherwise, Cyt-c and Cyt-D solutions were prepared in 10 mM PBS, pH 7.0, at 25 °C.

2.6. Circular dichroism

CD spectra measurements were conducted with a Jasco J-815 spectropolarimeter and were collected in the far-UV (260–200 nm) region. The experiments were performed on Cyt-D samples prepared in 20 mM Tris/HCl buffer, and placed in a 1 mm cell at 25 °C.

3. Results and discussion

3.1. Cyt-D stability

R. marinus is a thermophile bacterium with ca. 65–70 °C optimal growth temperature; hence implying that its terminal caa_3 oxygen reductase complex is thermally stable within this temperature range in the native environment. Cyt-D, however, is only a soluble domain

fragment of subunit II and, thus, lacks native contacts with the remaining enzyme complex that may be essential to attain high stability. Therefore we investigated the stability of Cyt-D towards thermal and chemical denaturation employing different spectroscopic methods that provide complementary structural information at the levels of the heme active site and surrounding protein matrix, respectively.

The UV-CD spectrum of ferric Cyt-D recorded at room temperature and neutral pH displays the typical features of a well folded C-type protein mainly composed of α-helical secondary structural elements, with two negative bands at 208 and 220 nm (Fig. 1) [21]. Upon increasing the temperature from 20 to 90 °C the intensity of these features is gradually lost, particularly at 220 nm, exhibiting a single transition with apparent melting temperature $T_m = 59 \pm 2$ °C. Thus, the thermal stability of Cyt-D is comparable to soluble C-type cytochromes from mesophiles, which usually present T_m values between 60 and 80 °C [3,8], but lower than for other proteins from thermophilic organisms such as the soluble cytochrome *c* from *R. marinus*, for which the reported T_m value is 106 °C [22].

These results indicate that indeed, in spite of being a stable and well folded protein, the isolated Cyt-D domain lacks essential contacts responsible for providing exceptionally high thermal stability. Consistent with this interpretation, when the protein is cross-linked to electrodes coated with mixed self-assembled monolayers (SAMs) of C_{15}-CH_3 and C_{15}-COOH employing CMC and NHS, the SERR spectrum of the immobilized Cyt-D remains essentially unaltered up to 75 °C (the highest temperature achievable with the experimental set-up), thus suggesting that protein–SAM interactions mimic to a certain extent the native protein–protein contacts that provide extended thermal stability (Fig. S1). The stabilization of Cyt-D upon immobilization on SAM-coated electrodes hints at the potential suitability of this redox protein for the design of bioelectronics devices.

To further characterize the stability of Cyt-D, we also evaluated its sensitivity towards a commonly used chemical denaturant agent, guanidine hydrochloride (GuHCl). The addition of GuHCl results in a blueshift of the Soret absorption band (Fig. S2) that is characterized by a low amplitude transition at a GuHCl midpoint concentration of ca. $C_m(1) = 0.1$ M and a second large amplitude and sharp transition at $C_m(2) = 4.7$ M (Fig. 2A). UV–vis absorption spectra of cytochromes are very sensitive to the oxidation state and ligation of the heme iron, as well as to the hydration and polarity of the heme pocket [23–26]. Most likely the first transition corresponds to a minor population of less well folded protein or to the formation of an intermediate state in the unfolding pathway that still preserves the axial coordination pattern. For the second transition the larger shift of the Soret maximum to 400 nm, which further shifts to 398 nm upon lowering pH, suggests the replacement of the Met axial ligand [26]. Indeed, resonance Raman (RR) spectra recorded at high GuHCl concentrations (Fig. S3) are consistent with a 6-coordinated low spin heme with either Lys/His or H_2O/His axial coordination pattern [26]. Moreover, RR spectra of Cyt-D recorded in the presence of variable concentrations of GuHCl from 0 to 6 M can be consistently simulated by superposition of only two RR spectral components, i.e. native Cyt-D and the above mentioned Lys/His or H_2O/His species, using only their relative contributions as adjustable parameters (Fig. S4). This treatment yields the titration curve shown in Fig. 2C, from where, in contrast to the UV–vis experiments, a single and broad transition with $C_m = 3.0$ M is obtained. Monitoring of the GuHCl titration by the disappearance of the 220 nm band of the CD spectrum also reveals a single and relatively broad transition with $C_m = 2.9$ M, i.e. very similar to the RR results (Figs. S5 and 2B). Control GuHCl titrations of horse heart Cyt-c performed under similar conditions afford a single transition with $C_m = 2.9$ M (Fig. S6), in good agreement with previous UV–vis, CD and RR determinations for this and other soluble cytochromes [27,28]. Thus, the results suggest a different unfolding mechanism for Cyt-D compared to Cyt-c, although the overall sensitivity to GuHCl appears to be comparable.

It is well established that the interactions of GuHCl with the peptide functional group are crucial for destabilizing the protein structure [29–31]. A number of studies assign these interactions as H-bonding to the peptide carbonyl [30,32–35], although more recent work points out to stacking rather than H-bonding [36]. Moreover, it has been proposed that GuHCl is a particularly effective denaturant of helical peptides when the stability is strongly influenced by the presence of planar amino acid side chains [37], and less efficient if stabilization is mainly due to salt bridges [38].

The GuHCl-induced loss of helical content in Cyt-D is revealed by CD spectroscopy as a gradual process characterized by a transition that is broader than for Cyt-c, in spite of the fact that the C_m values are similar. This may indicate a different distribution of planar amino acid side chains as crucial stabilizing elements in Cyt-D. In contrast, the rupture

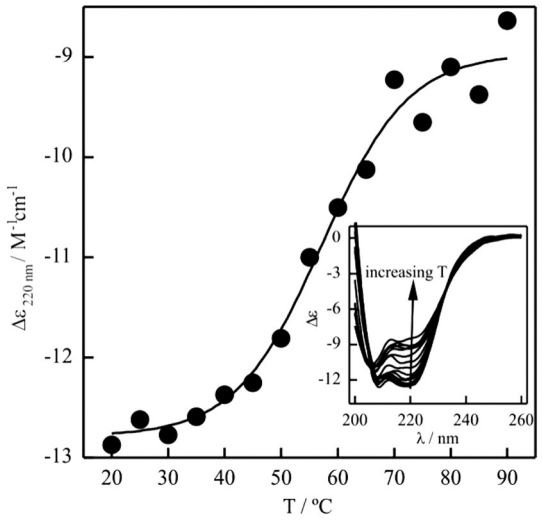

Fig. 1. Temperature dependence of the ellipticity of ferric Cyt-D at 220 nm recorded at neutral pH. Inset: UV-CD spectra of Cyt-D as a function of temperature.

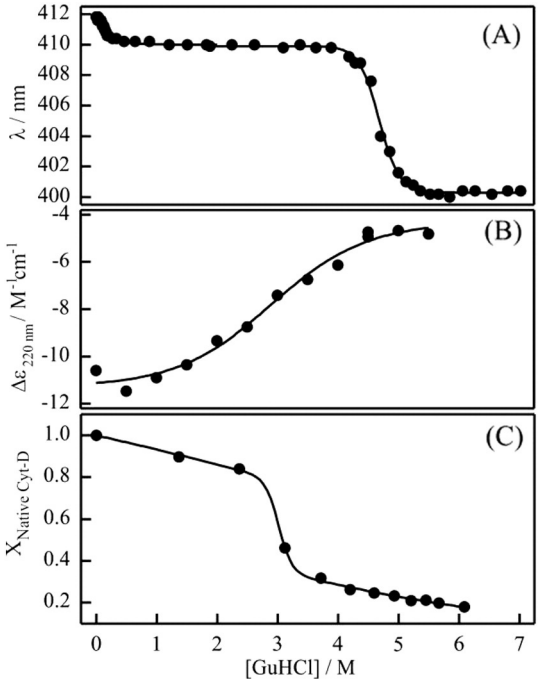

Fig. 2. Cyt-D denaturation by GuHCl as monitored by: (A) the position of the Soret absorption band ($C_m(1) = 0.1$ M and $C_m(2) = 4.7$ M); (B) UV-CD at 220 nm ($C_m = 2.9$ M) and (C) component analysis of the resonance Raman spectra ($C_m = 3.0$ M). $X_{Native\ Cyt\text{-}D}$ is the mole fraction of Cyt-D that retains the native conformation.

of the (Met)S–Fe bond is revealed by UV–vis absorption as a sharp transition at higher GuHCl concentrations, thereby suggesting a higher stability of the heme pocket in Cyt-D.

A close inspection of the protein structures shows that the total content of residues with planar side chains is 15 and 16 for Cyt-D and Cyt-c, respectively. The number of these residues located in α helices is also comparable: 6 and 5, respectively. An important difference, however, is that in the case of Cyt-c one of these residues, Tyr67, is hydrogen bonded to the axial ligand Met80 and, therefore, has been identified as a crucial element for stabilizing the native structure [39]. Thus, the perturbation of Tyr67 by GuHCl can be expected to trigger the simultaneous loss of α-helical content and the rupture of the (Met)S–Fe bond in Cyt-c. Moreover, perturbation of the nearby Tyr74 in the same helix is likely to promote similar events. Cyt-D, in contrast, lacks tyrosine residues at hydrogen bonding distances with respect to the axial ligands, which may explain the observed differences in unfolding behavior between the two cytochromes.

In summary, we conclude that the thermal stability of isolated Cyt-D is comparable to canonical cytochromes but, in contrast to Cyt-c [40], the thermal stability of Cyt-D increases upon immobilization on SAM-coated electrodes. In addition, the heme active site of Cyt-D exhibits higher stability towards chemical denaturants such as GuHCl.

3.2. Alkaline transition

Soluble cytochromes *c* from different organisms exhibit a pH-dependent structural transition with pK_a around 9 from the native form (or state III) to the alkaline form (or state IV) in which the native axial ligand methionine is replaced by a lysine residue, thus yielding a Lys/His axial coordination pattern. Upon further increase of pH a second transition to the so-called state V is typically observed with pKa ~ 11, which involves significant protein unfolding and the replacement of the lysine axial ligand by OH^- [3,8].

We investigated this transition for Cyt-D by employing UV–vis absorption and CD spectroscopy to follow the acid–base titrations. In the first case we monitored the disappearance of the charge transfer band at 695 nm as indicative of the rupture of the (Met)S–Fe bond (Fig. S7), while in the second case the intensity drop at 220 nm was employed to monitor the loss of alpha-helical content (Fig. S8). As shown in Fig. 3, both spectroscopic methods yield identical results, i.e. $pK_a = 11.7$. This value is well above the pKa determined for the first alkaline transition of Cyt-c (Fig. S9), and close to the pKa of the subsequent IV → V transition [3,8]. Thus, the high pK_a value and the fact that the rupture of the (Met)S–Fe bond occurs concomitantly with the loss of the secondary structure elements suggest that protein unfolding occurs before a conventional alkaline transition (in terms of Met/Lys replacement) can take place.

In good agreement with this interpretation, RR spectra measured at various pH values can be consistently simulated by convolution of only two spectral components: the RR spectrum of native Cyt-D and a second species with spectral parameters consistent with a low spin iron with OH^-/His axial coordination (Fig. 4A) [26,41]. A plot of the relative intensities of these two spectral components yields $pK_a = 12.2$, i.e. very close to the values obtained by CD and UV–vis (Fig. 4B).

3.3. Thermodynamic and kinetic redox parameters

The thermodynamic redox properties of Cyt-D were investigated by cyclic voltammetry and SERR spectroelectrochemistry. For this purpose, the protein was adsorbed on Au or Ag electrodes, respectively, coated with SAMs of 1:1 C_{11}-OH/C_{10}-CH_3, which have been shown to be suitable for efficient adsorption of Cyt-D [17]. SERR measurements as a function of the applied electrode potential show that the adsorbed protein can be quantitatively reduced and oxidized in a reversible manner and, moreover, the spectra of the fully reduced and fully oxidized Cyt-D are identical to the corresponding RR spectra in solution (Fig. S10). Note that these spectroelectrochemical measurements were performed under Soret-band excitation which, in contrast to previous Q-band experiments [17], allow for the sensitive detection of native and non-native cytochrome species in both redox states [26,40,41]. As we do not detect SERR spectral components other than those corresponding to ferrous and ferric native Cyt-D in solution, the present results indicate that more than 95% of the adsorbed protein retains the solution

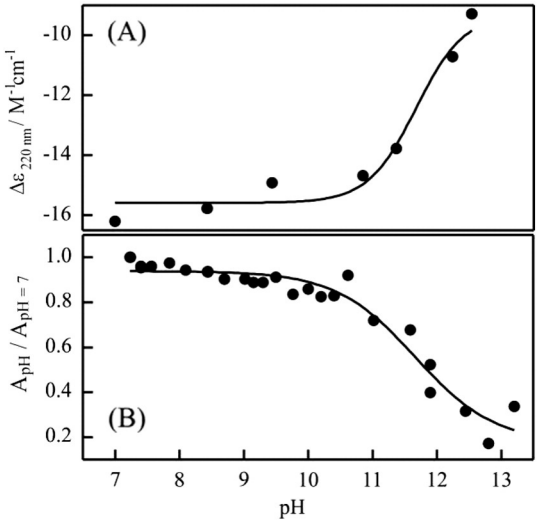

Fig. 3. Acid–base titration of Cyt-D as monitored by the drop of the CD band at 220 nm (A) and of the charge transfer absorption band at 695 nm (B).

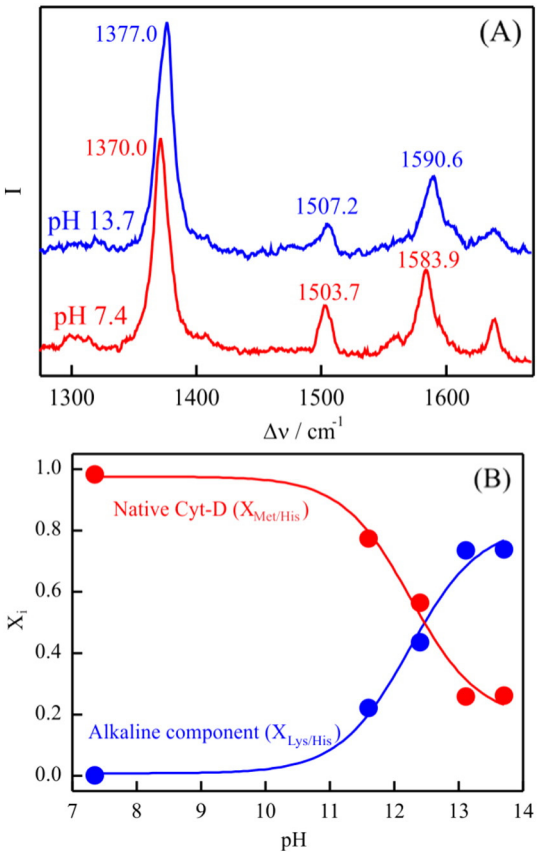

Fig. 4. (A) Resonance Raman spectra of Cyt-D recorded at neutral and alkaline pH. (B) Mole fractions of the native (Met/His) and alkaline (OH^-/His) Cyt-D conformers determined from the resonance Raman spectral components as a function of pH.

structure at the level of the heme pocket. The component analysis of SERR spectra determined as a function of the applied potential allows for the quantitative determination of relative surface concentrations of the reduced and oxidized species. This analysis yields nearly ideal Nernst plots for a one electron reaction with a standard reduction potential of $E^0 = 58 \pm 3$ mV vs. Ag/AgCl (Fig. S11), in very good agreement with previous determinations in solution and in biomimetic complexes [15,17].

CV determinations of Cyt-D adsorbed on SAM-coated electrodes at neutral pH and room temperature (Fig. S12) reveal a linear dependence of E^0 with the ionic strength of the solution (Fig. 5A) that can be treated in terms of the extended Debye–Hückel model:

$$E^0 = E^* - 0.059A\left(Z_{ox}^2 - Z_{red}^2\right) f(I) \quad (1)$$

where $f(I) = \sqrt{I}/\left(1 + Ba\sqrt{I}\right)$; E^* is the standard reduction potential at zero ionic strength, Z_{ox} and Z_{red} are the charges of the oxidized and reduced species; I is the solution ionic strength; A depends on the relative permittivity and temperature and has a value of 0.509 $(L/mol)^{1/2}/cm$ at 25 °C; $B = 0.329 \times 10^8$ $(L/mol)^{1/2}/cm$ at 25 °C and $a = 18$ Å is the effective radius [42].

The results shown in Fig. 5A yield a protein charge of $Z_{red} = +1.6$. Considering that pKa values of individual amino acids may be affected by the specific environment, this experimental value is very close to the zero order estimate, $Z_{red} = +1$, obtained by simply computing the formal charges of the heme group and of the surface residues from their pKa values in solution at neutral pH.

The thermodynamic parameters for the redox reaction of Cyt-D were determined by CV from the temperature-dependence of the formal redox potential at neutral pH (Figs. 5B and S13). Within the experimental temperature range 5–35 °C the electrochemical cell behaves as perfectly non-isothermal. Thus, entropy and enthalpy changes associated to the redox reaction can be extracted from the slope of the plot in Fig. 5B according to:

$$\Delta S = nF\left(\frac{\partial E}{\partial T}\right) \quad (2)$$

$$\Delta H = nF\left[T\left(\frac{\partial E}{\partial T}\right) - E\right]. \quad (3)$$

This treatment yields $\Delta S = -135$ kJ mol^{-1}, which suggests that the oxidized form of Cyt-D is entropically favored with respect to the reduced species. Most likely such stabilization arises from increased protein rigidity in the reduced state determined due to differences in the hydrogen bonding network rather than due to solvation effects, as the heme redox center is only marginally exposed to the solvent. At physiologically relevant temperatures, the entropic term is compensated by a negative enthalpic term, $\Delta H = -45$ kJ mol^{-1}, that can be rationalized in terms of stabilization of the ferrous form by ligand binding interactions and by the hydrophobicity of the heme pocket. Negative ΔS values have been found for all C-type cytochromes studied so far with values ranging from ca. −15 to −150 J K^{-1} mol^{-1}, while ΔH values commonly encountered are between −30 and −80 kJ mol^{-1} [43]. So, enthalpy–entropy compensation in protein ET is not a peculiarity of Cyt-D.

The reduction potential shows only a slight and gradual decrease with increasing pH that represents only 50 mV over 6 pH units, with an apparent pK_a value well above 10 (Fig. 5C). This behavior is not consistent with a Met/Lys exchange of the iron axial ligand, as this process is expected to produce ca. 300 to 500 mV downshifts of the E^0 values [43]. Instead, the small and gradual decrease of E^0 suggests only partial unfolding of the protein without disruption of the (Met)S–Fe bond within the experimentally accessible pH range, in agreement with the results presented in the previous sections.

To determine the ET reorganization energy (λ), we performed TR-SERR spectroelectrochemical experiments on Cyt-D samples adsorbed on Ag electrodes coated with SAMs of C_{20}-OH/C_{19}-CH_3 in 3:1 ratio. In this technique the redox protein equilibrated at a given initial electrode potential is perturbed by applying potential jumps of variable amplitude that corresponds to varying overpotentials (η) and, therefore, different ET driving forces. The heterogeneous ET kinetics is monitored by recording SERR spectra at various delay times with respect to the triggering potential jump event. Therefore, the election of thicker SAMs for the kinetic experiments aims to warrant that the determined reaction rates correspond to a process limited by electron tunneling probability through the SAM [44].

Representative TR-SERR spectra are shown in Fig. S14. The complete spectral data set could be quantitatively simulated by using only the spectral components of native ferrous and ferric Cyt-D in variable proportions. This analysis yields in all cases monoexponential concentration profiles, from where the ET rate constants at the various overpotentials, $k_{ET}(\eta)$, were obtained. The determined rate constants exhibit the sigmoidal dependence with η predicted by Marcus semiclassical expression properly integrated to account for all the electronic levels of the metal (Fig. 6) [45]. This equation can be cast in a more conventional form by approximating the Fermi–Dirac distribution law as a step function:

$$k_{ET}(\eta) \approx \frac{\pi}{\hbar}|H_{DA}|^2 erfc\left(\frac{\lambda + e\eta}{\sqrt{4\lambda k_B T}}\right). \quad (4)$$

Here $|H_{DA}|$ is the magnitude of the electronic coupling, erfc(z) is the reciprocal error function and the rest of the parameters have the usual

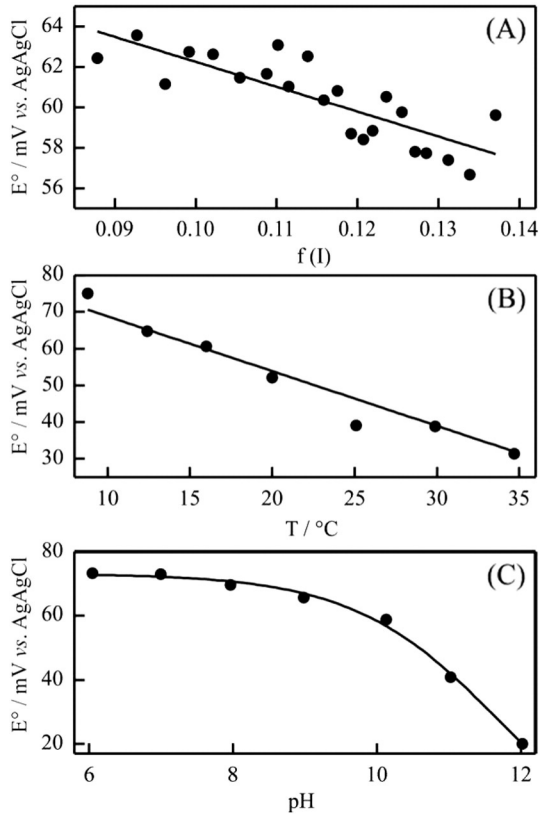

Fig. 5. Variation of the formal reduction potential of Cyt-D with ionic strength function $f(I) = \sqrt{I}/\left(1 + Ba\sqrt{I}\right)$ at room temperature and neutral pH (A), with temperature at neutral pH (B), and with pH at room temperature (C). The working electrodes were coated with SAMs of 1:1 C_{11}-OH/C_{10}-CH_3. All potentials are quoted versus the Ag/AgCl (3.5 M KCl) reference electrode.

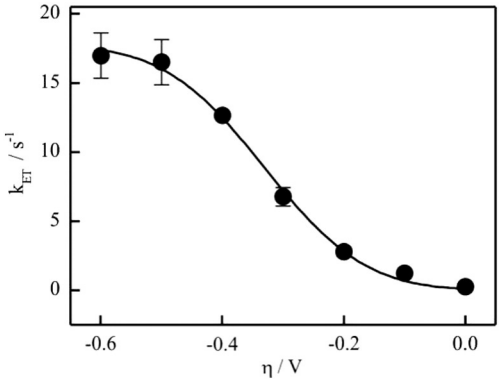

Fig. 6. Rate constants of heterogeneous electron transfer of adsorbed Cyt-D as a function of the applied overpotential in the time-resolved surface-enhanced resonance Raman (TR-SERR) experiments. The line represents the best fit to Eq. (4), yielding $\lambda = 0.33$ eV and $k_{ET}(max) = 17.7\ s^{-1}$. All the experiments were performed at neutral pH and room temperature. The working electrodes were coated with SAMs of 1:1 C_{20}–OH/C_{19}–CH_3.

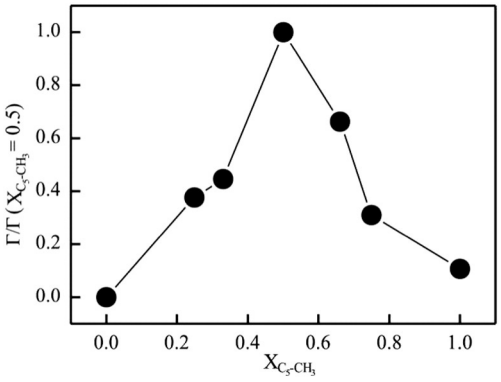

Fig. 7. Surface concentration (Γ) of HiPIP adsorbed on Au electrodes coated with SAMs of C_5-CH_3/ C_6-OH of variable proportion as a function of the mole fraction of the C_5-CH_3 component. The values of Γ were estimated by integration of the cyclic voltammetric peaks and are presented normalized by the value obtained for a SAM with composition $X_{C_5-CH_3} = 0.5$.

meaning. By fitting the experimental data in Fig. 6 to Eq. (4) we obtain $\lambda = 0.33 \pm 0.03$ eV. Due to the fact that this value was obtained under Soret band excitation, it is considered to be more precise than the one reported in an earlier communication [17], where less sensitive Q-band excitation was employed. Note that the SERR cross section is significantly smaller for Q-band excitation compared to Soret band, particularly for the ferric protein.

Reorganization energies reported in the literature for cytochromes *c* from different organisms, or even for the very same heme protein, exhibit a large dispersion. In a recent study this dispersion was rationalized in terms of a crucial structural feature: those cytochromes which possess a tyrosine residue H-bonded to the axial ligand methionine have on average $\lambda = 0.6$ eV; while in those cases where an equivalent H-bond is not possible or it is interrupted by electrostatic interactions the average λ value is only 0.3 eV [39]. The value of $\lambda = 0.33$ eV determined here for Cyt-D is fully consistent with this interpretation as this protein, in contrast to mammalian or yeast Cyt-c, does not have a Tyr or other appropriate residues in H-bonding distance to the axial methionine [15].

3.4. Redox properties of the putative electron donor of Cyt-D

Previous studies have identified a 10 kDa soluble $[4Fe–4S]^{3+/2+}$ protein as the most likely electron shuttle from a bc_1 analog complex to the caa_3 oxygen reductase in the aerobic respiratory chain of *R. marinus* [13,15,18]. We have investigated this HiPIP protein by direct CV in solution employing gold electrodes coated with SAMs of C_6-OH. The recorded voltammetries exhibit the characteristic shape and scan rate dependence for a quasi-reversible one electron redox couple in solution (Fig. S15), yielding $E° = 55 \pm 3$ mV vs. Ag/AgCl at pH 7, in excellent agreement with previous determinations [18]. The pH-dependence of $E°$ is only 4 mV/pH unit within the range 4–11, and becomes slightly more sensitive at even lower pH values (Fig. S16).

HiPIP has been proposed to interact with Cyt-D via complementary neutral patches defined by hydrophobic and hydrophilic residues surrounding the partially exposed redox centers, thereby establishing optimal electron transfer pathways [15,17]. To test this hypothesis we investigated the adsorption of HiPIP to Au electrodes coated with mixed SAMs of C_5-CH_3 and C_6-OH in variable proportions. For these experiments the coated electrodes were incubated overnight in 25 μM protein solutions, then rinsed and transferred to the electrochemical cell containing fresh PBS, pH 7. The relative surface concentration of HiPIP was estimated from the integrated voltammetric peaks measured under identical conditions. As shown in Fig. 7 the protein adsorption reaches a maximum at C_5-CH_3/C_6-OH ratios of ca. 1:1, and is negligible at SAMs of the single components, thus indicating that the adsorption requires a balance of hydrophobic and hydrophilic interactions. Interestingly, this behavior is nearly identical to the one previously reported for Cyt-D [17], thereby confirming the complementarity of the proposed binding sites.

The reduction potential and its pH-dependence for HiPIP adsorbed and in solution are very similar (Figs. S16 and S17), thus indicating that the immobilized protein retains the native structure, at least at the level of the redox center. Therefore, we determined the heterogeneous electron transfer rate constants of HiPIP immobilized on Au electrodes coated with 1:1 C_n-CH_3/C_{n+1}-OH SAMs of variable lengths, i.e. n = 3, 5, 7, 10 and 15, using Laviron's method [46]. As shown in Fig. S18, shortening the SAM length from n = 15 to n = 10 results in a ca. 200-fold increase of k_{ET}, which is consistent with a redox reaction kinetically controlled by tunneling probability through the SAM, with a tunneling decay factor $\beta = 1.0$ per methylene group, in excellent agreement with previous determinations [47,48]. Further decreasing of the SAM thickness results only in a slight increase of k_{ET}, thus revealing a different ET mechanism at shorter distances, as extensively discussed in the literature for other redox proteins [44]. Hence, we selected C_{15}-CH_3/C_{16}-OH SAMs for obtaining the ET activation parameters of HiPIP from the temperature-dependence of k_{ET} (Fig. 8). These experiments yield the ET activation enthalpy $\Delta H^{\#}$ which, considering that the entropic contribution in redox proteins is usually very small, can be approximated to the activation free energy $\Delta G^{\#}$. In turn, according to Marcus theory, $\Delta G^{\#} = \lambda/4$ when $\Delta G° = 0$. Within this approximation, we obtain $\lambda = 0.42 \pm 0.03$ eV. This value lies within the range 0.2–0.9 eV of previous experimental and theoretical estimates of reorganization energies for [4Fe–4S] proteins [49–54].

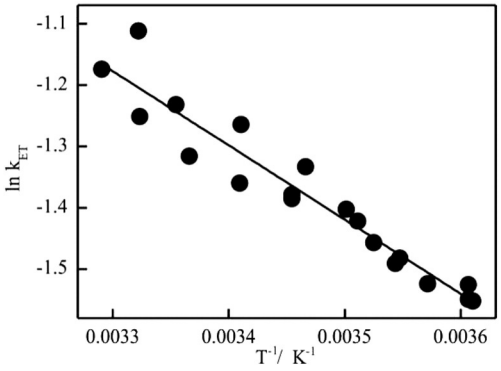

Fig. 8. Temperature-dependence of the heterogeneous electron transfer rate of HiPIP adsorbed on SAM-coated Au electrodes (1:1 C_{20}-OH/C_{19}-CH_3). The values of k_{ET} were determined by CV using Laviron's method [46].

3.5. Electrocatalytic activity of Cyt-D

Several pentacoordinated heme proteins, including microperoxidases, horse radish peroxidases and point mutant cytochromes *c*, exhibit electrocatalytic activity towards H_2O_2 reduction and have, therefore, been employed for the construction of H_2O_2 electrode sensors [55–61]. Potential drawbacks of these sensors, however, are the possible oxidative damage and bleaching of the porphyrin ring, depending on the specific heme protein and H_2O_2 concentration [62], as well as partial denaturation upon immobilization [40]. In this respect, the higher stability of Cyt-D discussed in the previous sections might represent an intrinsic advantage for the construction of these types of devices. To further assess this potential advantage, we compared the bleaching of the heme groups of Cyt-D and Cyt-c in solution as a function of H_2O_2 concentration. The experiments were performed by adding successive aliquots of H_2O_2 to 10 μM solutions of the two proteins in 10 mM PBS pH 7, and following the progress of the reaction by UV–vis (Fig. S19). As shown in Fig. 9A, the Soret band of Cyt-c is quantitatively bleached at H_2O_2 concentrations around 80 mM, while the intensity drop for Cyt-D under identical conditions is only 40%.

Moreover, the addition of 1 mM H_2O_2 to 10 μM Cyt-c produces 50% bleaching of the heme after 40 min, while the same amount of oxidant has nearly no effect on the absorption spectrum of Cyt-D even after 7 h, and the addition of 20 mM H_2O_2 to 10 μM Cyt-D requires around 8 h to produce 50% bleaching (Figs. 9B and S20). Thus, these experiments show a significantly higher stability of Cyt-D towards degradation by H_2O_2.

In view of its high thermal and chemical stability, we tested the pseudoperoxidatic activity of Cyt-D adsorbed on Au electrodes coated with mixed SAMs of C_{10}-CH_3/C_{11}-OH in 1:1 ratio.

The CVs show the characteristic one-electron anodic and cathodic waves of native Cyt-D with $E^0 = 48 \pm 3$ mV, along with increasing catalytic currents at negative potentials upon addition of H_2O_2 (Fig. 10A). In agreement with previous reports on comparable systems [58,63], control experiments with protein free SAM-coated electrodes show only negligible currents upon addition of H_2O_2 up to ca. 100 mM concentration (Fig. 10B), thus indicating that the electrocatalytic currents arise from the immobilized Cyt-D. The activity, however, cannot be ascribed to the Met/His-coordinated native Cyt-D given that the onset of the catalytic currents is significantly downshifted with respect to the standard potential. Instead, most likely, the catalytic currents arise from a minor population of adsorbed Cyt-D that lacks the distal Met74 ligand. Such pentacoordinated species are expected to present standard potentials at around −400 mV or less, and significant pseudoperoxidase activities, as shown for instance for horse radish peroxidase [57] and M80A mutants of Cyt-c [58].

As shown in Fig. 10B, there is a short initial lag phase before catalytic currents become evident. This is consistent with the requirement of a H_2O_2-mediated activation step to generate the enzymatically competent species. In recent work it has been shown that the addition of H_2O_2 to immobilized horse heart Cyt-c leads to the specific sulfoxidation of Met80 and concomitant gain of pseudoperoxidase activity [55]. Most likely the same applies to Cyt-D, except that in this latter case the chemical yield of the reaction is very low, in agreement with the differences in reactivity between Cyt-D and Cyt-c shown in Fig. 9. Thus, we propose that the catalytic activity corresponds to a minor fraction of adsorbed Cyt-D that presents a pentacoordinated heme iron due to sulfoxidation of Met74. These results suggest that Cyt-D may be a suitable building block for the design of electrochemical biosensors.

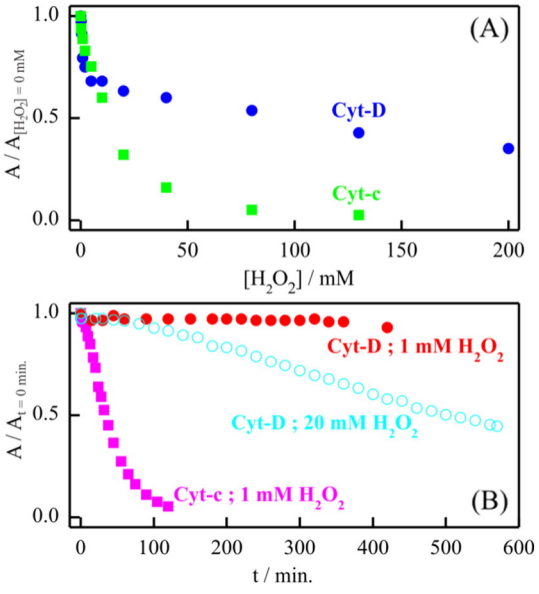

Fig. 9. Normalized absorbance at 411 nm of 10 μM solutions of Cyt-D (circles) and Cyt-c (squares) in 10 mM PBS, pH 7.0. (A) Variation as a function of H_2O_2 concentration determined immediately after H_2O_2 addition. (B) Variation as a function of time after addition of H_2O_2 to achieve 1 mM (filled symbols) and 20 mM (hollow symbols) final concentrations. All data are presented relative to the initial absorbances recorded before the addition of H_2O_2.

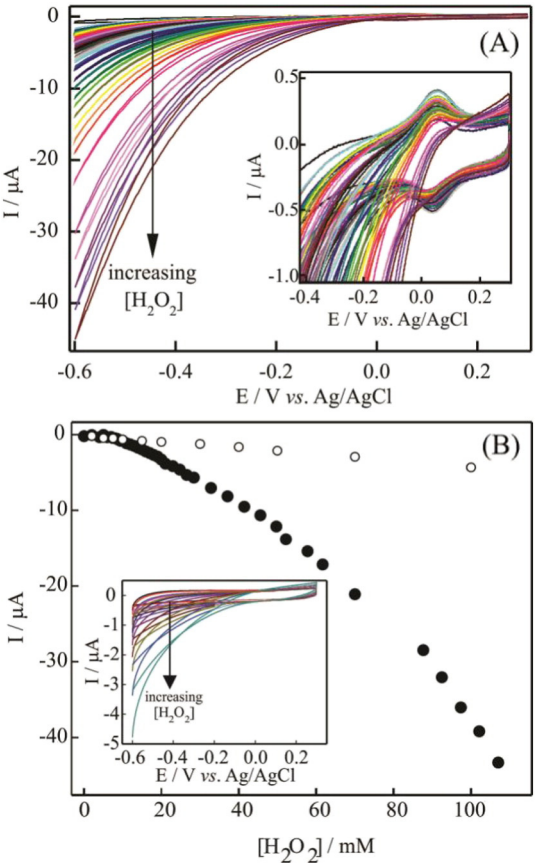

Fig. 10. (A) Cyclic voltammetries of Cyt-D adsorbed on Au electrodes coated with C_{10}-CH_3/C_{11}-OH, as a function of H_2O_2 concentration (10 mM PBS, pH 7). The inset is an expanded view of the voltammetric peaks of Cyt-D. (B) Electrocatalytic currents recorded at -600 mV as a function of H_2O_2 concentration from CV experiments with Au electrodes coated with C_{10}-CH_3/C_{11}-OH without (hollow circles) and with (solid circles) adsorbed Cyt-D. The inset shows typical CVs recorded with protein free SAM-coated electrodes as a function of H_2O_2 concentration from 0 to 100 mM. All potentials are quoted versus the Ag/AgCl (3.5 M KCl) reference electrode.

4. Conclusions

The soluble cytochrome *c* domain (Cyt-D) from the *R. marinus* caa_3 terminal oxygen reductase shows a thermal stability comparable to

C-type soluble cytochromes from mesophiles, but this stability increases significantly when the protein is immobilized on SAM-coated electrodes. The heme pocket shows superior stability towards chemical denaturation, alkaline transition and oxidative bleaching compared to archetypical cytochromes, which is further increased when adsorbed on biomimetic electrodes. Moreover, the immobilized protein retains the solution structure and exhibits fast direct heterogeneous electron transfer characterized by a low reorganization energy, $\lambda = 0.3$ eV, consistent with the lack of hydrogen bonding at the level of the iron axial ligand methionine.

Cyt-D and its putative electron donor HiPIP exhibit similar affinity for SAM-coatings containing identical proportions of hydrophobic and hydrophilic tail groups. As for Cyt-D, the immobilization of HiPIP on these films preserves the structural integrity of the redox site and allows for fast direct electron transfer with $\lambda = 0.6$ eV, thus suggesting that Cyt-D and HiPIP contain complementary binding sites capable of establishing efficient pathways for inter-protein electron transfer.

The high stability and good direct electrochemical communication of immobilized Cyt-D make this protein a suitable candidate for constructing protein-based sensing devices. Indeed, the Cyt-D electrodes show good electrocatalytic activity towards H_2O_2 reduction in a broad range of concentrations.

Acknowledgments

We thank Dr. Smilja Todorovic and Prof. Miguel Teixeira (ITQB-Portugal) for kindly providing the protein samples.

The financial support from ANPCyT (PICT2010-70 and 2011-1249) and UBA (UBACyT 20020130100206BA) to DHM is gratefully acknowledged. MAC and DHM are members of CONICET. LB is recipient of a CIN fellowship.

Appendix A. Supplementary data

Supplementary data to this article can be found online at http://dx.doi.org/10.1016/j.bioelechem.2015.05.005.

References

[1] I. Bertini, G. Cavallaro, A. Rosato, Cytochrome c: occurrence and functions, Chem. Rev. 106 (2006) 90–115.
[2] E.B. Sawyer, P.D. Barker, Continued surprises in the cytochrome c biogenesis story, Protein Cell 3 (2012) 405–409.
[3] G.R. Moore, G.W. Pettigrew, Cytochromes c. Evolutionary, Structural and Physicochemical Aspects, Springer-Verlag, Berlin-Heidelberg-New York, 1990.
[4] A.V. Kulikov, E.S. Shilov, I.A. Mufazalov, V. Gogvadze, S.A. Nedospasov, B. Zhivotovsky, Cytochrome c: the Achilles' heel in apoptosis, Cell. Mol. Life Sci. 69 (2012) 1787–1797.
[5] M. Huttemann, P. Pecina, M. Rainbolt, T.H. Sanderson, V.E. Kagan, L. Samavati, J.W. Doan, I. Lee, The multiple functions of cytochrome c and their regulation in life and death decisions of the mammalian cell: from respiration to apoptosis, Mitochondrion 11 (2011) 369–381.
[6] Y.L.P. Ow, D.R. Green, Z. Hao, T.W. Mak, Cytochrome c: functions beyond respiration, Nat. Rev. Mol. Cell Biol. 9 (2008) 532–542.
[7] J. Liu, S. Chakraborty, P. Hosseinzadeh, Y. Yu, S. Tian, I. Petrik, A. Bhagi, Y. Lu, Metalloproteins containing cytochrome, iron–sulfur, or copper redox centers, Chem. Rev. 114 (2014) 4366–4369.
[8] Cytochrome c: A Multidisciplinary Approach, in: R.A. Scott, A.G. Mauk (Eds.), University Science Books, Sausalito, 1996.
[9] C.M. Soares, A.M. Baptista, M.M. Pereira, M. Teixeira, Investigation of protonatable residues in *Rhodothermus marinus* caa_3 haem-copper oxygen reductase: comparison with *Paracoccus denitrificans* aa_3 haem–copper oxygen reductase, J. Biol. Inorg. Chem. 9 (2004) 124–134.
[10] H. Sigurdson, A. Namslauer, M.M. Pereira, M. Teixeira, P. Brzezinski, Ligand binding and the catalytic reaction of cytochrome caa_3 from the thermophilic bacterium *Rhodothermus marinus*, Biochemistry 40 (2001) 10578–10585.
[11] M. Santana, M.M. Pereira, N.P. Elias, C.M. Soares, M. Teixeira, Gene cluster of *Rhodothermus marinus* high-potential iron–sulfur protein: oxygen oxidoreductase, a caa_3-type oxidase belonging to the superfamily of heme–copper oxidases, J. Bacteriol. 183 (2001) 687–699.
[12] M.M. Pereira, M.L. Verkhovskaya, M. Teixeira, M.I. Verkhovsky, The caa_3 terminal oxidase of *Rhodothermus marinus* lacking the key glutamate of the D-channel is a proton pump, Biochemistry 39 (2000) 6336–6340.
[13] M.M. Pereira, M. Santana, C.M. Soares, J. Mendes, J.N. Carita, A.S. Fernandes, M. Saraste, M.A. Carrondo, M. Teixeira, The caa_3 terminal oxidase of the thermohalophilic bacterium *Rhodothermus marinus*: a HiPIP : oxygen oxidoreductase lacking the key glutamate of the D-channel, Biochim. Biophys. Acta Bioenerg. 1413 (1999) 1–13.
[14] M.M. Pereira, F.L. Sousa, M. Teixeira, R.M. Nyquist, J. Heberle, A tyrosine residue deprotonates during oxygen reduction by the caa_3 reductase from *Rhodothermus marinus*, FEBS Lett. 580 (2006) 1350–1354.
[15] V. Srinivasan, C. Rajendran, F.L. Sousa, A.M.P. Melo, L.M. Saraiva, M.M. Pereira, M. Santana, M. Teixeira, H. Michel, Structure at 1.3 angstrom resolution of *Rhodothermus marinus* caa_3 cytochrome c domain, J. Mol. Biol. 345 (2005) 1047–1057.
[16] A.F. Verissimo, F.L. Sousa, A.M. Baptista, M. Teixeira, M.M. Pereira, Thermodynamic redox behavior of the heme centers in A-type heme–copper oxygen reductases: comparison between the two subfamilies, Biophys. J. 95 (2008) 4448–4455.
[17] M.F. Molinas, A. De Candia, S.H. Szajnman, J.B. Rodríguez, M. Martí, M. Pereira, M. Teixeira, S. Todorovic, D.H. Murgida, Electron transfer dynamics of *Rhodothermus marinus* caa_3 cytochrome c domains on biomimetic films, Phys. Chem. Chem. Phys. 13 (2011) 18088–18098.
[18] M. Stelter, A.M.P. Melo, G.O. Hreggvidsson, S. Hjorleifsdottir, L.M. Saraiva, M. Teixeira, M. Archer, Structure at 1.0 resolution of a high-potential iron–sulfur protein involved in the aerobic respiratory chain of *Rhodothermus marinus*, J. Biol. Inorg. Chem. 15 (2010) 303–313.
[19] J. Grochol, R. Dronov, F. Lisdat, P. Hildebrandt, D.H. Murgida, Electron transfer in SAM/Cytochrome/polyelectrolyte hybrid systems on electrodes: a time-resolved surface-enhanced resonance Raman study, Langmuir 23 (2007) 11289–11294.
[20] N. Wisitruangsakul, I. Zebger, K.H. Ly, D.H. Murgida, S. Ekgasit, P. Hildebrandt, Redox-linked protein dynamics of cytochrome c probed by time-resolved surface enhanced infrared absorption spectroscopy, Phys. Chem. Chem. Phys. 10 (2008) 5276–5286.
[21] S.M. Kelly, T.J. Jess, N.C. Price, How to study proteins by circular dichroism, Biochim. Biophys. Acta Protein Proteomics 1751 (2005) 119–139.
[22] M. Stelter, A.M.P. Melo, M.M. Pereira, C.M. Gomes, G.O. Hreggvidsson, S. Hjorleifsdottir, L.M. Saraiva, M. Teixeira, M. Archer, A novel type of monoheme cytochrome c: biochemical and structural characterization at 1.23 Å resolution of *Rhodothermus marinus* cytochrome c, Biochemistry 47 (2008) 11953–11963.
[23] E. Margoliash, A. Schejter, Cytochrome c, Adv. Protein Chem. 21 (1966) 113–286.
[24] A. Schejter, W.A. Eaton, Charge-transfer optical spectra, electron paramagnetic resonance, and redox potentials of cytochromes, Biochemistry 23 (1984) 1081–1084.
[25] R.F. Latypov, H. Cheng, N.A. Roder, J. Zhang, H. Roder, Structural characterization of an equilibrium unfolding intermediate in cytochrome c, J. Mol. Biol. 357 (2006) 1009–1025.
[26] S. Oellerich, H. Wackerbarth, P. Hildebrandt, Spectroscopic characterization of nonnative conformational states of cytochrome c, J. Phys. Chem. B 106 (2002) 6566–6580.
[27] J.A. Knapp, C.N. Pace, Guanidine hydrochloride and acid denaturation of horse, cow, and *Candida krusei* cytochromes c, Biochemistry 13 (1974) 1289–1294.
[28] S.R. Yeh, D.L. Rousseau, Ligand exchange during unfolding of cytochrome c, J. Biol. Chem. 274 (1999) 17853–17859.
[29] T.O. Street, D.W. Bolen, G.D. Rose, A molecular mechanism for osmolyte-induced protein stability, Proc. Natl. Acad. Sci. U. S. A. 103 (2006) 13997–14002.
[30] D.R. Robinson, W.P. Jencks, The effect of compounds of the urea-guanidinium class on the activity coefficient of acetyltetraglycine ethyl ester and related compounds, J. Am. Chem. Soc. 87 (1965) 2462–2470.
[31] E.S. Courtenay, M.W. Capp, R.M. Saecker, M.T. Record, Structural stability of binding sites: consequences for binding affinity and allosteric effects, Proteins Struct. Funct. Genet. 41 (2000) 63–71.
[32] E.P. O'Brien, R.I. Dima, B. Brooks, D. Thirumalai, Interactions between hydrophobic and ionic solutes in aqueous guanidinium chloride and urea solutions: lessons for protein denaturation mechanism, J. Am. Chem. Soc. 129 (2007) 7346–7353.
[33] P.E. Mason, J.W. Brady, G.W. Neilson, C.E. Dempsey, The interaction of guanidinium ions with a model peptide, Biophys. J. 93 (2007) L04–L06.
[34] G.I. Makhatadze, P.L. Privalov, Protein interactions with urea and guanidinium chloride; a calorimetric study, J. Mol. Biol. 226 (1992) 491–505.
[35] M.L. Tiffany, S. Krimm, Extended conformations of polypeptides and proteins in urea and guanidine hydrochloride, Biopolymers 12 (1973) 575–587.
[36] W.K. Lim, J. Rosgen, S.W. Englander, Urea, but not guanidinium, destabilizes proteins by forming hydrogen bonds to the peptide group, Proc. Natl. Acad. Sci. U. S. A. 106 (2009) 2595–2600.
[37] C.E. Dempsey, T.J. Piggot, P.E. Mason, Dissecting contributions to the denaturant sensitivities of proteins, Biochemistry 44 (2005) 775–781.
[38] J.S. Smith, J.M. Scholtz, Guanidine hydrochloride unfolding of peptide helices: separation of denaturant and salt effects, Biochemistry 35 (1996) 7292–7297.
[39] D. Alvarez-Paggi, M.A. Castro, V. Tortora, L. Castro, R. Radi, D.H. Murgida, Electrostatically driven second-sphere ligand switch between high and low reorganization energy forms of native cytochrome c, J. Am. Chem. Soc. 135 (2013) 4389–4397.
[40] D.H. Murgida, P. Hildebrandt, Electron-transfer processes of cytochrome c at interfaces. New insights by surface-enhanced resonance Raman spectroscopy, Acc. Chem. Res. 37 (2004) 854–861.
[41] S. Dopner, P. Hildebrandt, F.I. Resell, A.G. Mauk, Alkaline conformational transitions of ferricytochrome c studied by resonance Raman spectroscopy, J. Am. Chem. Soc. 120 (1998) 11246–11255.
[42] J. Petrovic, R.A. Clark, H. Yue, D.H. Waldeck, E.F. Bowden, Impact of surface immobilization and solution ionic strength on the formal potential of immobilized cytochrome c, Langmuir 21 (2005) 6308–6316.

[43] G. Battistuzzi, M. Borsari, M. Sola, F. Francia, Redox thermodynamics of the native and alkaline forms of eukaryortic and bacterial class I cytochromes c, Biochemistry 36 (1997) 16247–16258.
[44] H. Khoa Ly, M. Sezer, N. Wisitruangsakul, J.J. Feng, A. Kranich, D. Millo, I.M. Weidinger, I. Zebger, D.H. Murgida, P. Hildebrandt, Surface-enhanced vibrational spectroscopy for probing transient interactions of proteins with biomimetic interfaces: electric field effects on structure, dynamics and function of cytochrome c, FEBS J. 278 (2011) 1382–1390.
[45] R.A. Marcus, On theory of electron-transfer reactions. Unified treatment for homogeneous and electrode reactions, J. Chem. Phys. 43 (1965) 679–701.
[46] E. Laviron, General expression of the linear potential sweep voltammogram in the case of diffusionless electrochemical systems, J. Electroanal. Chem. 101 (1979) 19–28.
[47] D.H. Murgida, P. Hildebrandt, Redox and redox-coupled processes of heme proteins and enzymes at electrochemical interfaces, Phys. Chem. Chem. Phys. 7 (2005) 3773–3784.
[48] B. Liu, A.J. Bard, M.V. Mirkin, S.E. Creager, Electron transfer at self-assembled monolayers measured by scanning electrochemical microscopy, J. Am. Chem. Soc. 126 (2004) 1485–1492.
[49] L.I. Krishtalik, The medium reorganization energy for the charge transfer reactions in proteins, Biochim. Biophys. Acta Bioenerg. 1807 (2011) 1444–1456.
[50] D. Mitra, V. Pelmenschikov, Y. Guo, D.A. Case, H. Wang, W. Dong, M.L. Tan, T. Ichiye, F.E. Jenney, M.W.W. Adams, Y. Yoda, J. Zhao, S.P. Cramer, Dynamics of the [4Fe–4S] cluster in *Pyrococcus furiosus* $D^{14}C$ ferredoxin via nuclear resonance vibrational and resonance raman spectroscopies, force field simulations, and density functional theory calculations, Biochemistry 50 (2011) 5220–5235.
[51] E. Sigfridsson, M.H.M. Olsson, U. Ryde, Inner-sphere reorganization energy of iron–sulfur clusters studied with theoretical methods, Inorg. Chem. 40 (2001) 2509–2519.
[52] R. Kummerle, J. Gaillard, P. Kyritsis, J.M. Moulis, Intramolecular electron transfer in [4Fe–4S] proteins: estimates of the reorganization energy and electronic coupling in *Chromatium vinosum* ferredoxin, J. Biol. Inorg. Chem. 6 (2001) 446–451.
[53] K.P. Jensen, Iron–sulfur clusters: why iron? J. Inorg. Biochem. 100 (2006) 1436–1439.
[54] E. Babini, I. Bertini, M. Borsari, F. Capozzi, C. Luchinat, X. Zhang, G.L.C. Moura, I.V. Kurnikov, D.N. Beratan, A. Ponce, A.J. Di Bilio, J.R. Winkler, H.B. Gray, Bond-mediated electron tunneling in ruthenium-modified high-potential iron–sulfur protein, J. Am. Chem. Soc. 122 (2000) 4532–4533.
[55] D.A. Capdevila, W.A. Marmisollé, F. Tomasina, V. Demichelli, M. Portela, R. Radi, D.H. Murgida, Specific methionine oxidation of cytochrome c in complexes with zwitterionic lipids by hydrogen peroxide: potential implications for apoptosis, Chem. Sci. 6 (2015) 705–713.
[56] J.J. Feng, P. Hildebrandt, D.H. Murgida, Silver nanocoral structures on electrodes: a suitable platform for protein-based bioelectronic devices, Langmuir 24 (2008) 1584–1586.
[57] B. Wang, J.J. Zhang, Z.Y. Pan, X.Q. Tao, H.S. Wang, A novel hydrogen peroxide sensor based on the direct electron transfer of horseradish peroxidase immobilized on silica-hydroxyapatite hybrid film, Biosens. Bioelectron. 24 (2009) 1141–1145.
[58] S. Casalini, G. Battistuzzi, M. Borsari, C.A. Bortolotti, G. Di Rocco, A. Ranieri, M. Sola, Electron transfer properties and hydrogen peroxide electrocatalysis of cytochrome c variants at positions 67 and 80, J. Phys. Chem. B 114 (2010) 1698–1706.
[59] S. Águila, A.M. Vidal-Limón, J.B. Alderete, M. Sosa-Torres, R. Vázquez-Duhalt, Unusual activation during peroxidase reaction of a cytochrome c variant, J. Mol. Catal. B Enzymatic 85–86 (2013) 187–192.
[60] G. Battistuzzi, M. Bellei, C.A. Bortolotti, M. Sola, Redox properties of heme peroxidases, Arch. Biochem. Biophys. 500 (2010) 21–36.
[61] A. Ranieri, F. Bernini, C.A. Bortolotti, E. Castellini, The Met80Ala point mutation enhances the peroxidase activity of immobilized cytochrome c, Catal. Sci. Technol. 2 (2012) 2206–2210.
[62] B. Valderrama, M. Ayala, R. Vazquez-Duhalt, Suicide inactivation of peroxidases and the challenge of engineering more robust enzymes, Chem. Biol. 9 (2002) 555–565.
[63] L. Wang, D.H. Waldeck, Denaturation of cytochrome c and its peroxidase activity when immobilized on SAM films, J. Phys. Chem. C 112 (2008) 1351–1356.

Supplementary Information

Stability, Redox Parameters and Electrocatalytic Activity of a Cytochrome Domain from a New Subfamily

María F. Molinas, Leandro Benavides, María A. Castro, and Daniel H. Murgida*

Departamento de Química Inorgánica, Analítica y Química Física and INQUIMAE (CONICET-UBA), Facultad de Ciencias Exactas y Naturales, Universidad de Buenos Aires, Ciudad Universitaria, Pab. 2, piso 1, C1428EHA-Buenos Aires, Argentina; E-mail: dhmurgida@qi.fcen.uba.ar

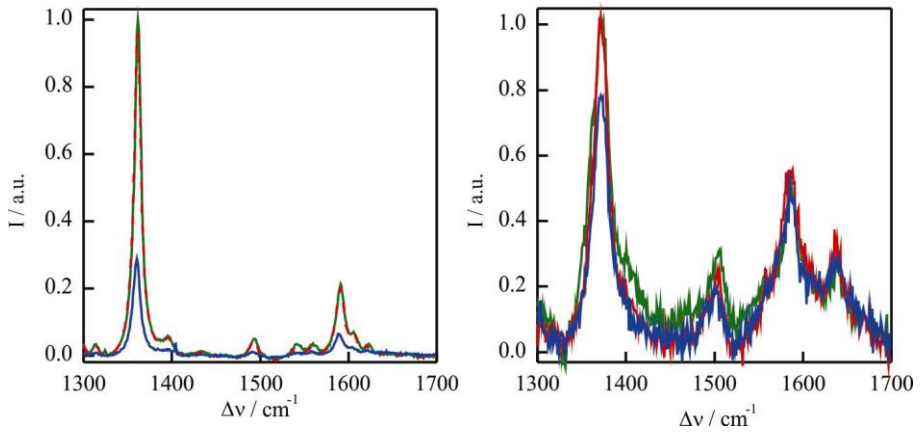

Figure S1. Surface-enhanced resonance Raman spectra of ferrous (left) and ferric (right) Cyt-D cross-linked to Ag electrodes coated with mixed SAMs of C_{15}-CH_3 / C_{15}-COOH recorded at different temperatures. Green: 10 °C. Red: 40°C. Blue: 75 °C.

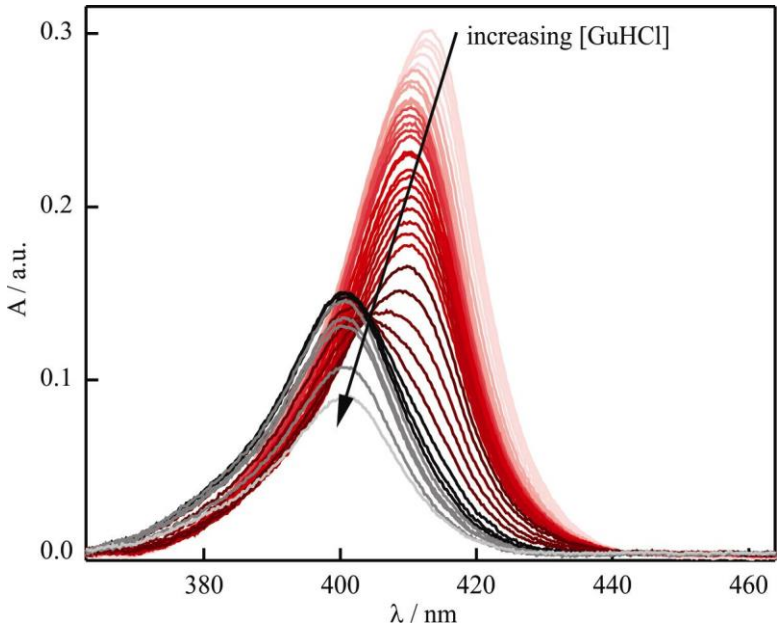

Figure S2. Soret absorption band of Cyt-D recorded at increasing concentrations of GuHCl, from 0 to 6.6 M.

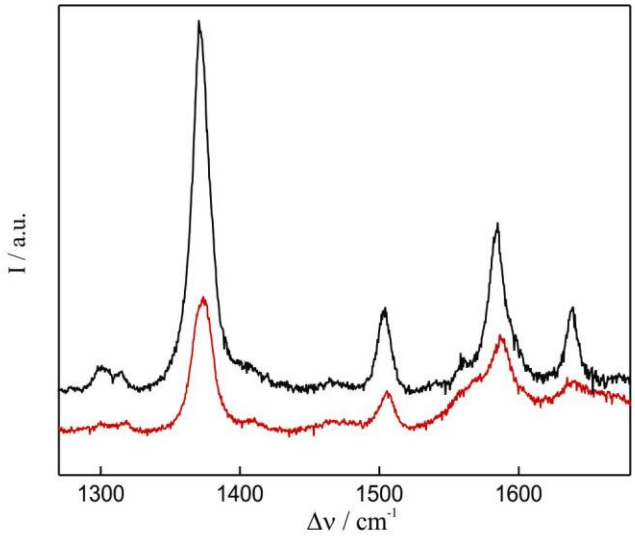

Figure S3. Resonance Raman spectra of Cyt-D measured at pH 7 under Soret-band excitation before (black) and after (red) the addition of 6 M GuHCl.

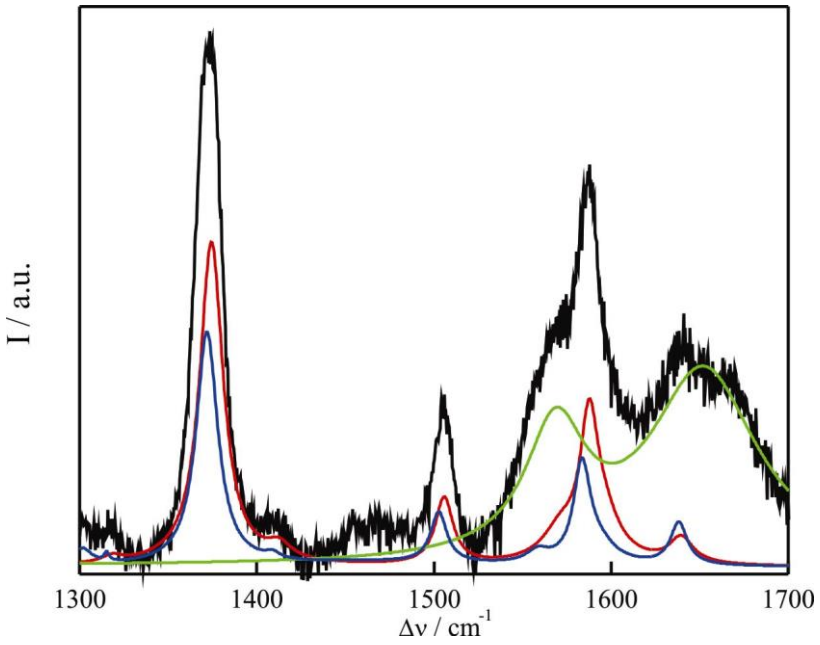

Figure S4. Experimental Resonance Raman spectrum of ferric Cyt-D in the presence of 6 M GuHCl (black) and the spectral components required to simulate the spectrum: native Cyt-D (red), His/Lys or His/H_2O ligated species (blue) and GuHCl (green).

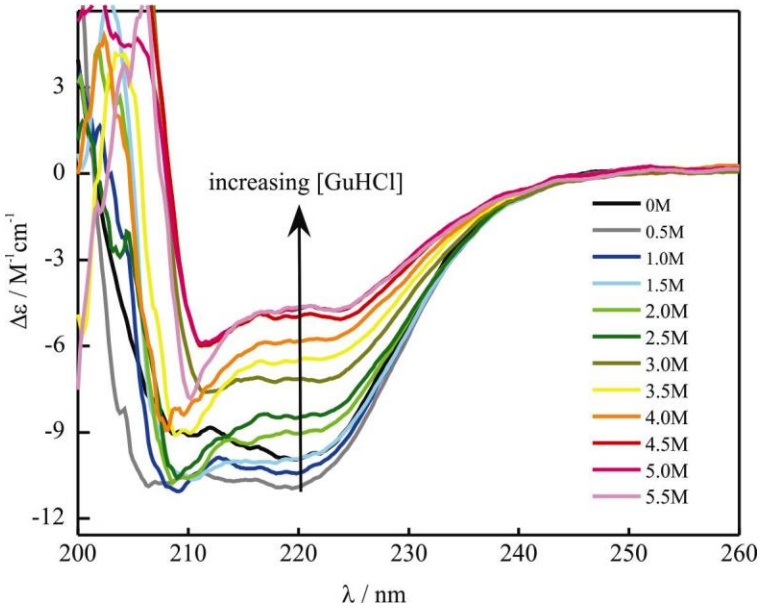

Figure S5. CD spectra of Cyt-D recorded at pH 7 as a function of GuHCl concentration.

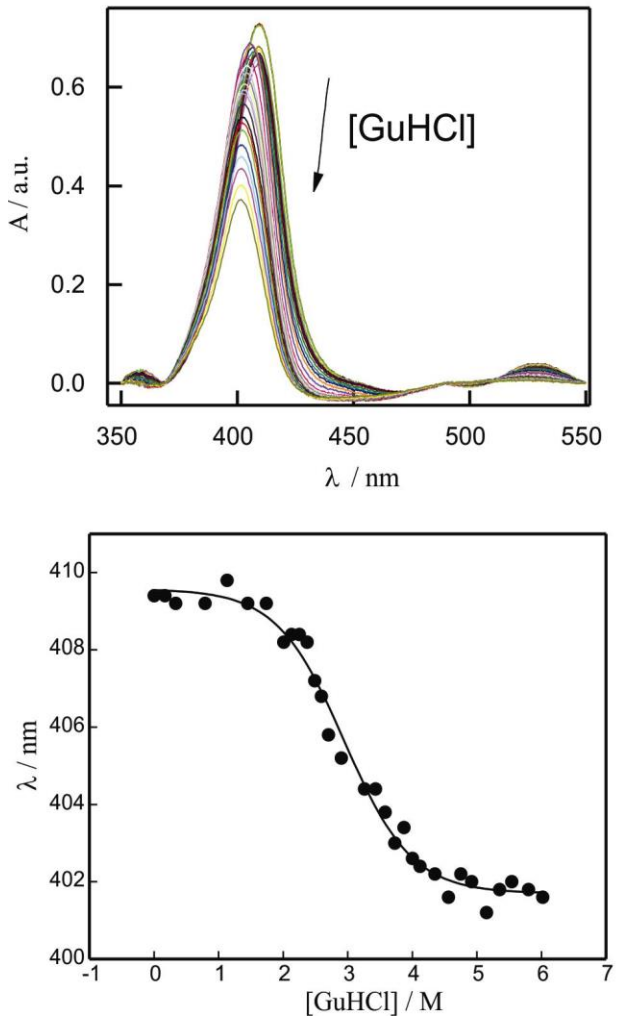

Figure S6. Denaturation of horse heart Cyt-c by GuHCl as monitored by the position of the Soret absorption band (C_m = 2.9 M).

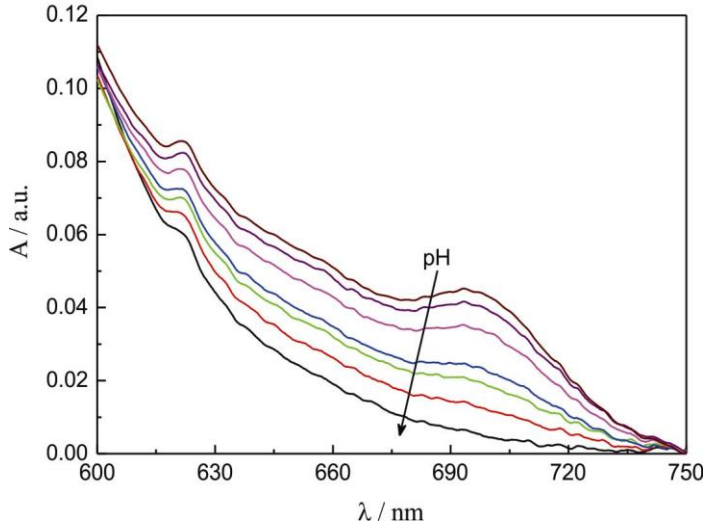

Figure S7. Acid-base titration of Cyt-D followed by the disappearance of the charge transfer band at 695 nm. The arrow indicates increasing pH values from 7 to 13.

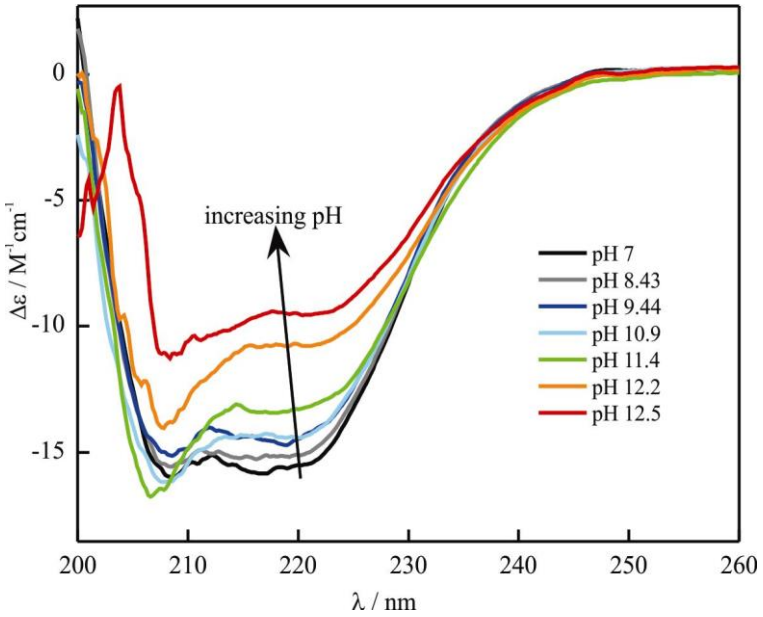

Figure S8. CD spectra of Cyt-D recorded as a function of pH.

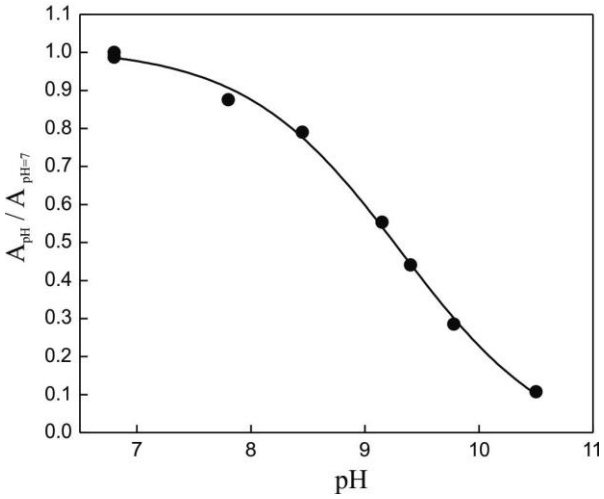

Figure S9. Acid-base titration of horse heart Cyt-c followed by the disappearance of the charge transfer band at 695 nm.

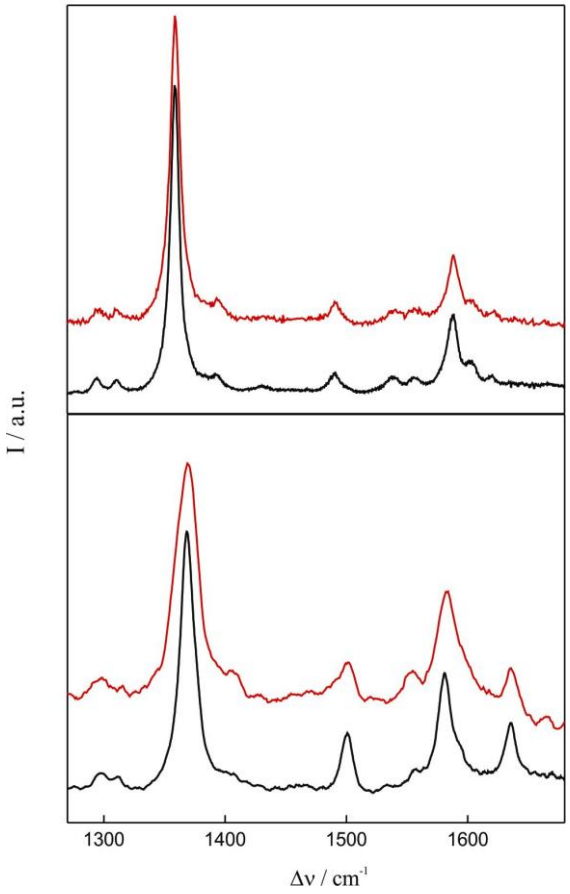

Figure S10. Resonance Raman (black) and surface-enhanced resonance Raman (red) spectra of fully reduced (top) and fully oxidized (bottom) Cyt-D measured at pH 7.0.

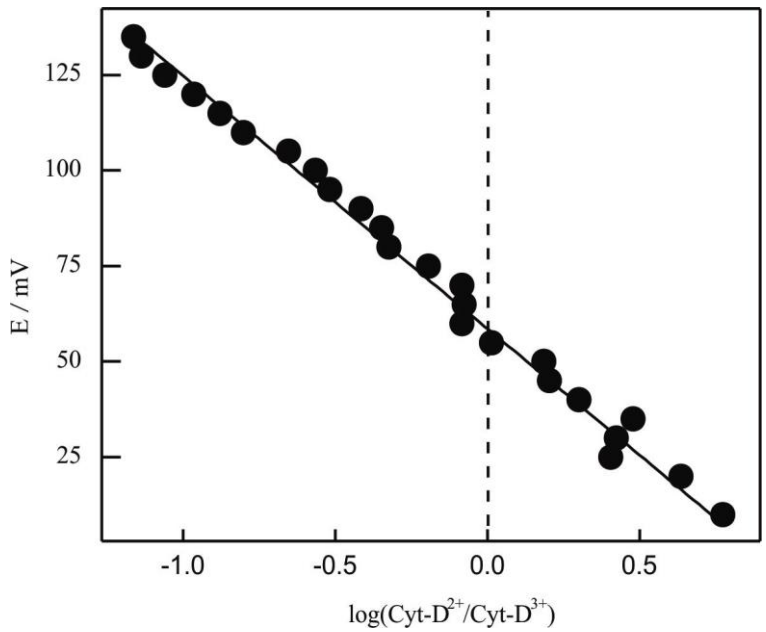

Figure S11. Nernst plot for Cyt-D adsorbed on an Ag electrode coated with a SAM of C_{11}-OH/C_{10}-CH_3 obtained from the quantitative component analysis of SERR recorded under Soret band excitation as a function of the electrode potential vs Ag/AgCl.

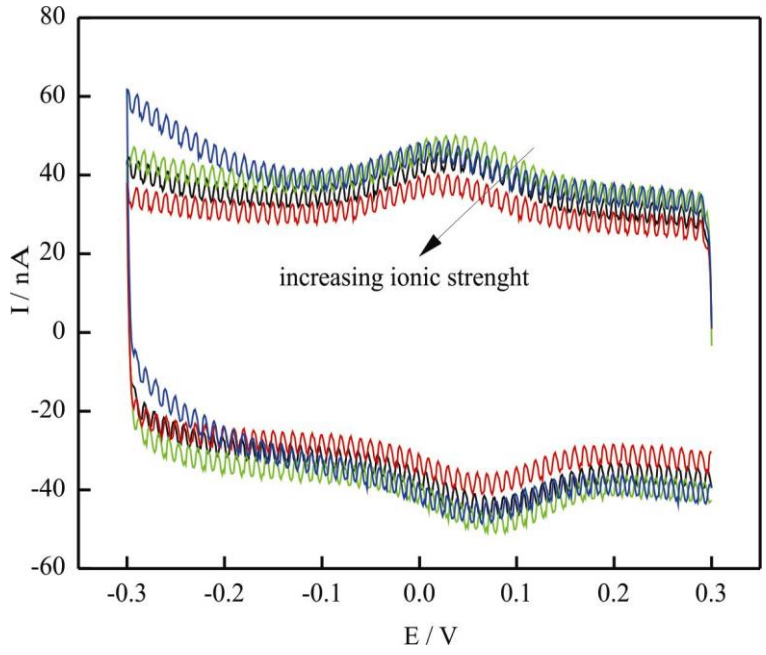

Figure S12. Cyclic voltammetry of Cyt-D adsorbed on Au electrodes coated with SAMs of C_{11}-OH/C_{10}-CH_3 measured at pH 7 vs Ag/AgCl and increasing ionic strength: 20 mM (green), 162 mM (black), 616 mM (red) and 1.6 M (blue).

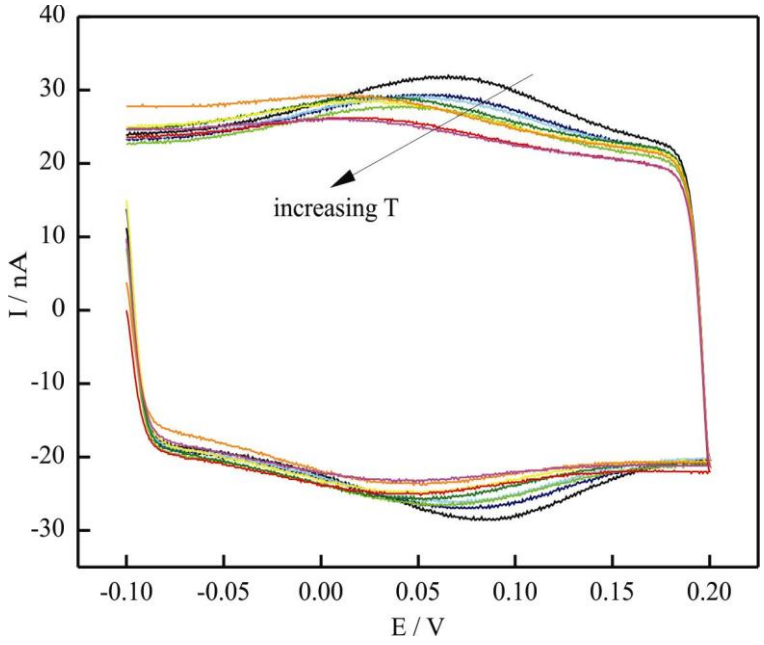

Figure S13. Cyclic voltammetry of Cyt-D adsorbed on Au electrodes coated with SAMs C_{11}-OH/C_{10}-CH_3 measured at pH 7 vs Ag/AgCl at increasing temperatures from 6 °C (black) to 44 °C (pink).

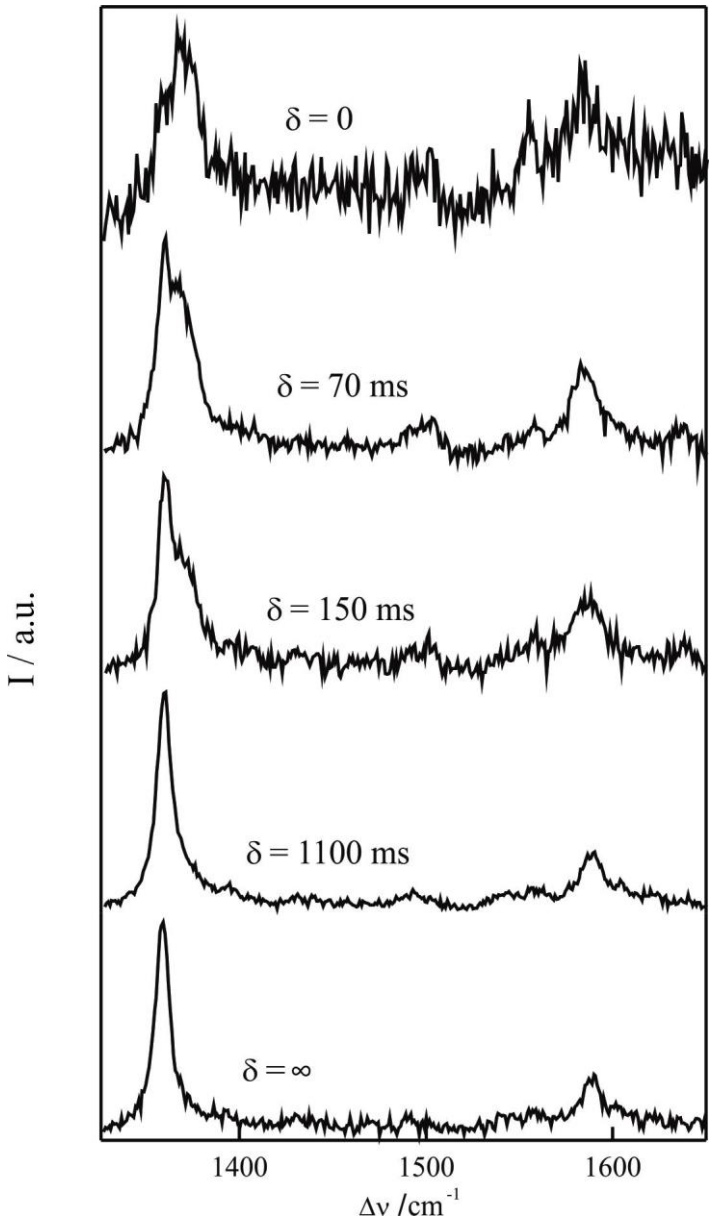

Figure S14. Representative time-resolved surface-enhanced resonance Raman spectra of Cyt-D adsorbed on Ag electrodes coated with SAMs of C_{20}-OH/C_{19}-CH_3 measured at pH 7 and room temperature. Spectra were recorded at variable delay times (δ) after applying potential jumps from 150 mV to -400 mV.

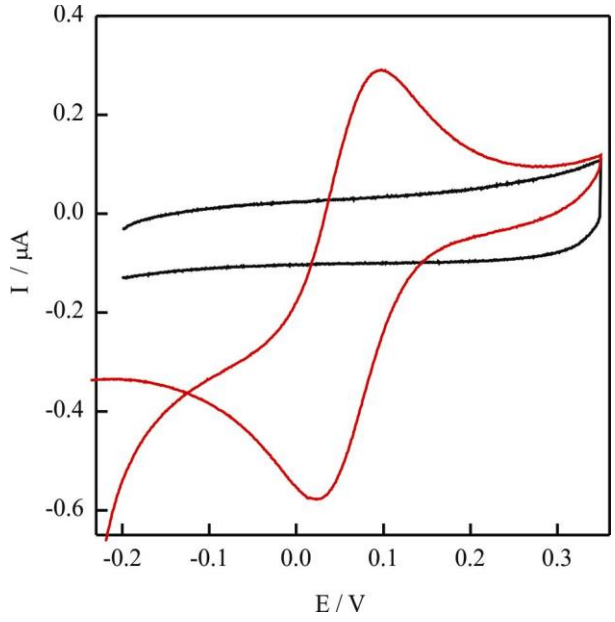

Figure S15. Cyclic voltammetry vs Ag/AgCl of HiPIP in solution (red) and control measurement of the Au working electrode coated with a SAM of C_6-OH in the absence of protein (black).

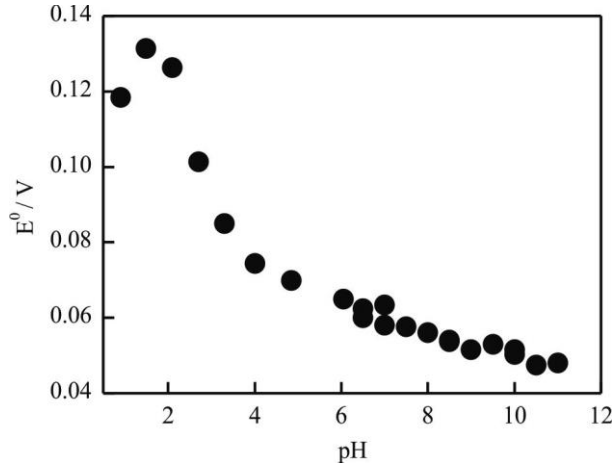

Figure S16. Variation of the formal reduction potential vs Ag/AgCl of HiPIP with pH, measured at room temperature by CV in solution using Au electrodes coated with C_6-OH SAMs.

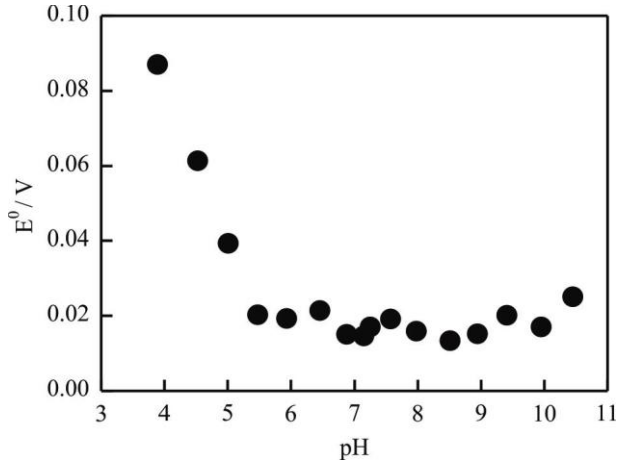

Figure S17. Variation of the formal reduction potential vs Ag/AgCl with pH for HiPIP adsorbed on Au electrodes coated with 1:1 C_5-CH_3 / C_6-OH SAMs, as determined by CV at room temperature.

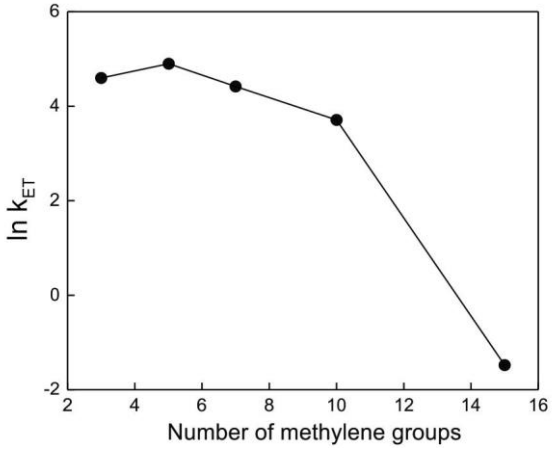

Figure S18. Heterogeneous electron transfer rate constants of HiPIP adsorbed on Au electrodes coated with 1:1 C_n-CH_3/C_{n+1}-OH SAMs, as a function of the chain length (n).

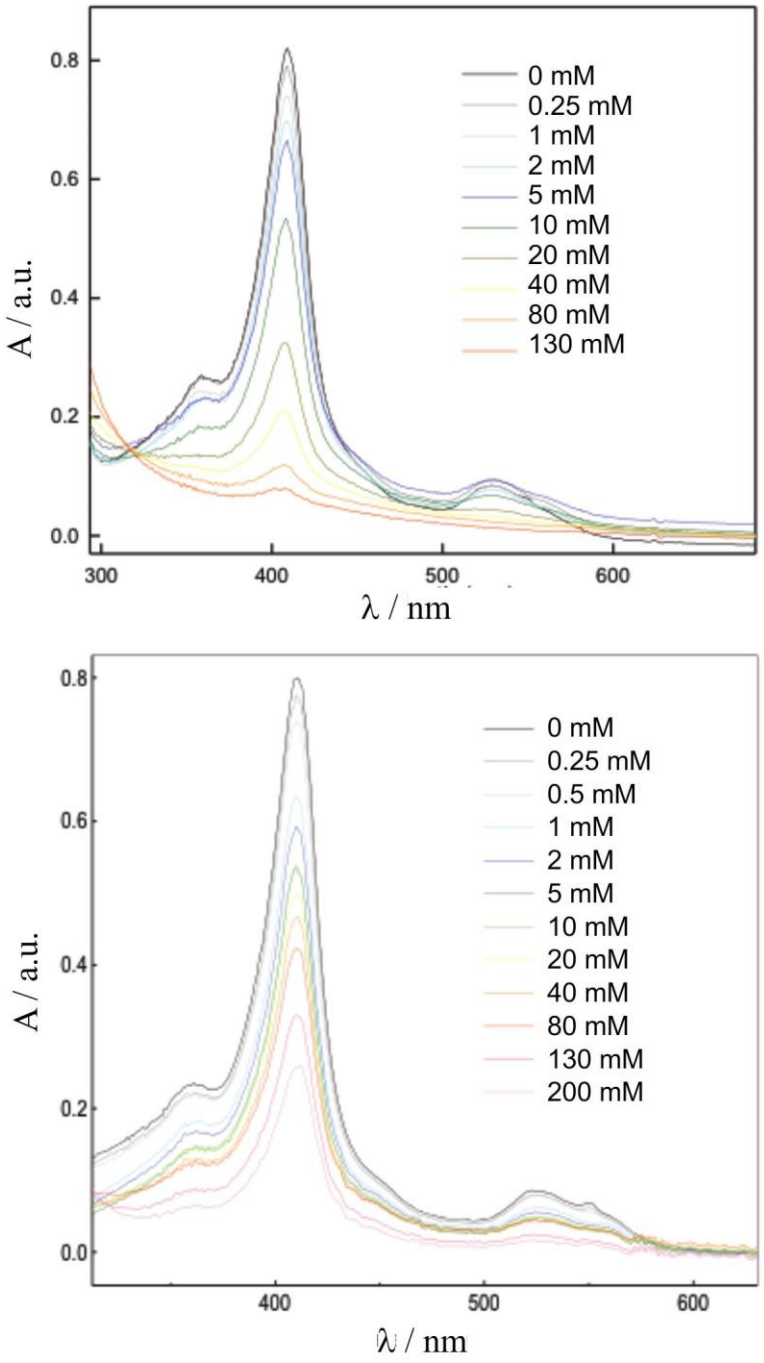

Figure S19. UV-Vis spectra of Cyt-c (top) and Cyt-D (bottom) recorded immediately after adding increasing amount of H_2O_2. The final concentrations of H_2O_2 are indicated in the corresponding panels.

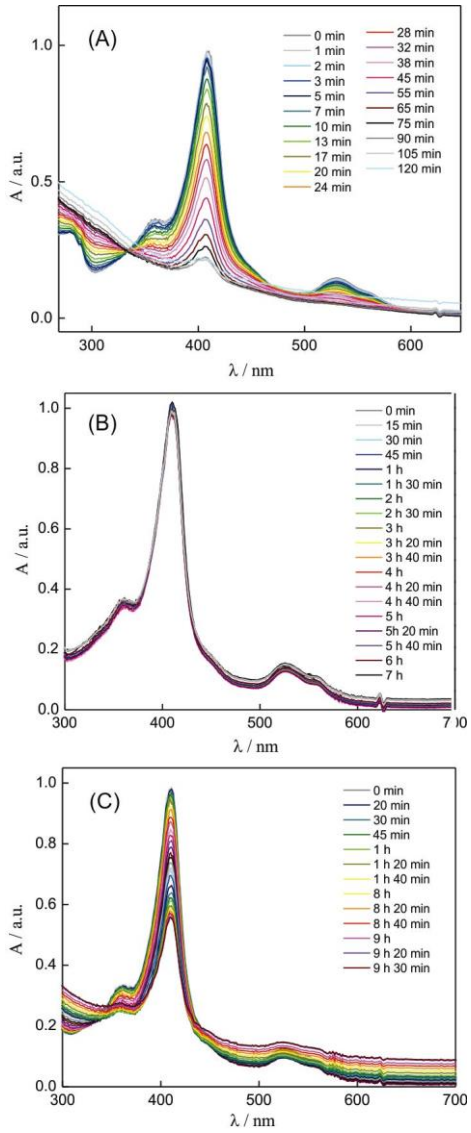

Figure S20. UV-Vis spectra measured as a function of time after the addition of H_2O_2. (A) Cyt-c with 1 mM added H_2O_2. (B) Cyt-D with 1 mM added H_2O_2. (C) Cyt-D with 20 mM added H_2O_2.